 doi:10.20944/preprints201703.0056.v1

Ag/$MgAl_2O_4$nanoparticles Prepared by a Modified Hydrothermal for Photocatalytic Degradation of Methylene Blue

Zhengru Zhu *, Jinfeng Zhang and Weirong Li

Research Center of Hydrology and Water Source, School of City and Environmental Science,

Liaoning Normal University, Dalian, 116029, China

* to whom correspondence should be addressed

*Corresponding author.

Tel.: +86-411-8215-8364

Fax: +86-411-8215-8542

E-mail address:zhengruzhu@gmail.com

 doi:10.20944/preprints201703.0056.v1

Abstract

In the present work report, the $MgAl_2O_4$and the $Ag/MgAl_2O_4$ samples were successfully synthesized by the modified hydrothermal and the isovolumetric impregnation methods, respectively. The structural properties of the prepared samples were systematically characterized by XRD, SEM, TEM, DRS, XPS and et al techniques. The photocatalytic degradation of methylene blue by the $Ag/MgAl_2O_4$ and $MgAl_2O_4$ samples was comparatively studied under UV lamp irradiation. The results revealed that the prepared $Ag/MgAl_2O_4$ (pH=6) samples were the most active among the samples in photocatalytic of methylene blue. Under UV lamp irradiation, the $Ag/MgAl_2O_4$ (pH=6) photodegradation of methylene blue reached to 89.6% within 120 min. And the $Ag/MgAl_2O_4$ (pH=6) complex photocatalysts displayed a high photochemical stability under repeated irradiation. Repeated irradiate the $Ag/MgAl_2O_4$ (pH=6) compound, which indicated it had a high photochemical stability.

Keywords: $Ag/MgAl_2O_4$; characterization; activity; Photocatalytic degradation; Methylene blue

 doi:10.20944/preprints201703.0056.v1

1. Introduction

Synthetic dyes of organic compounds containing the molecular structure of the chromophore. According to their chromophore groups, they arecommonly classified intoazo, anthraquinone, indigoide, phthalo-cyanine, sulfur, and triphenylmethane derivatives [1]. Synthetic dyes not only used in textile printing and dyeing, but also widely used in papermaking, plastics, leather, rubber, coatings, printing ink, cosmetics, photographic materials, and other industries[2]. However, most of industries dyes are toxic, carcinogenic, and mutagenic, and have little biodegrade ability [3]. Moreover, the dye into the waste water caused serious environmental problems [4]. Some of the dyes, dye precursors, and dye degradation products have carcinogenic and degeneration. A variety of physical, chemical, and biological method shave been developed for the treatment of dye wastewater, but these conventional processes usually exist some shortcomings for purifying the wastewater [5]. Photocatalysis in degradation of organic pollutants is regarded as a green and low cost technology, and as a promising alternative method for photovoltaic cells [6-8].

$MgAl_2O_4$ spinel is a commonly used catalyst carrier for various chemical reactions such as methane oxidation, alkane reforming, and dehydrogenation, because of its high melting temperature, high chemical stability, and distinguished optical and dielectric properties [9, 10]. In order to improve their catalytic performance, $MgAl_2O_4$ materials are highly desired to be synthesized and assembled into certain nano structures with high specific surface areas.

Nowadays, many researchers have tried to increase the photocatalytic activity by different methods, such as by using grapheme [11], mordenite [12] and metal doping, for example: Pd [13], Sm [14], Pt [15] and Ag [16]. They have a narrow band gap. Therefore, they can be excited by UV light. The

Preprints (www.preprints.org) | NOT PEER-REVIEWED | Posted: 10 March 2017 doi:10.20944/preprints201703.0056.v1

remarkable advantages of supported noble metal catalysts are relatively high activity, mild process conditions, and better handling properties. The choice of an efficient support could significantly improve the activity, selectivity, recycling, and reproducibility of Ag catalyst systems.

In the present work, $MgAl_2O_4$ samples were obtained via a simple and economic hydrothermal method along with different pH values to vary their crystallinity as well as their surface states, then were employed as Ag catalyst supports. After systematic characterization of the samples and surface structures, $MgAl_2O_4$ and $Ag/MgAl_2O_4$ samples are investigated for the photocatalytic activity and the reaction mechanism for the photocatalytic degradation of methylene blue (MB) under UV irradiation.

2. Materials and methods

2.1. Preparation of catalysts

All the chemicals were reagent grade and used without further purification. Deionized water was used as a solvent. The $MgAl_2O_4$ nanoparticles were prepared by using a modified hydrothermal method. Typically, Mg $(NO_3)_2 \cdot 6H_2O$ and Al $(NO_3)_3 \cdot 9H_2O$ were dissolved in deionized water (100 mL). The molar ratio of Mg: Al is fixed at 1:2. The pH of the mixture was adjusted to 6 and 8 by slowly adding concentrated ammonia. When the pH value is 6 and 8, the mixture was put into a Teflon-lined stainless steel autoclave at 200 ℃ for 20 h. Then, the system was allowed to cool to room temperature naturally. The precipitate was washed twice or three times with deionized water and ethanol, respectively. After that, the precipitate was kept at 80 ℃ for 12 h for drying. Finally, the preparation of the nanoparticles was calcined in air for 5 h at 750 ℃. The white $MgAl_2O_4$ sample was obtained. And the samples named as S-6 and S-8, respectively.

Preprints (www.preprints.org) | NOT PEER-REVIEWED | Posted: 10 March 2017 doi:10.20944/preprints201703.0056.v1

The catalyst of $Ag/MgAl_2O_4$ with 1 wt. % of Ag was prepared by a conventional wet impregnation route [17]. $AgNO_3$ solution was used as the precursor. First, the catalyst was measured the saturated water quantity. Then, corresponding volume of the $AgNO_3$ solution was configured and drop wise into the catalyst. After evaporation, the catalyst was then dried at 100°C for 12 h upon heating in air and calcined at 400°C in air for 6 h followed by slow cooling under air atmosphere. Then gray $Ag/MgAl_2O_4$ powders were obtained. The sample named as Ag/S-6 and Ag/S-8, respectively.

2.2. Characterizations

X-ray diffraction (XRD) pattern was recorded for the prepared $MgAl_2O_4$and$Ag/MgAl_2O_4$ powder from the 2θ range of 10 – 80° with a step of 0.02°by X-ray diffraction (XRD, RIGAKU, Dmax22000) with Cu Kα radiation (λ=0.15418 nm) and 30 mA current and 40 kV voltage was applied to the X-ray tube.

The prepared nanocrystalline $MgAl_2O_4$ and $Ag/MgAl_2O_4$ samples were previously degassed at 150°C for 2 h in vacuum to determine the specific surface area of these samples by the adsorption method under nitrogen gas at liquid nitrogen (LN_2) temperature (77K) on a Micromeritics ASAP-2000 equipment using a Brunauer-Emmet-Teller (BET) (Quantochrome, USA).Ultraviolet-Visible diffuse reflectance spectra between 200 and 800 nm (DRS, Shamazu-UV-240) of the products were collected. Fourier transform infrared spect rumof the samples was recorded in the range 4000–400 cm^{-1} using a‘Bruker Vertex 70’spectrophotometer with 4 cm^{-1} resolution. The morphology and existence of elements O, Mg and Al in the prepared nanocrystalline $MgAl_2O_4$ and $Ag/MgAl_2O_4$ samples were investigated by scanning electronic microscopy (SEM) with a JSM-6700 LV electron microscope operating at 5.0 kV and transmission electron microscope (TEM, FEI Tecnai G220). XPS data were recorded using a

Preprints (www.preprints.org) | NOT PEER-REVIEWED | Posted: 10 March 2017 doi:10.20944/preprints201703.0056.v1

Perkin-Elmer PHI 5600 electron spectrometer by acrochromatic Al Kα radiation (1486.6 eV) with Ar^+ sputtering to remove the surface layer of the samples.

2.3. Photocatalytic experiments of the $MgAl_2O_4$and $Ag/MgAl_2O_4$ catalysts

The photocatalytic activity of the catalysts was evaluated by the concentration of methylene blue (MB) under irradiation of a125 W with UV lamp (19 $mW \cdot cm^{-2}$, HPL-N125W, Philips (China)).50 mg photocatalyst powder was added into 100 mL 20 $mg \cdot L^{-1}$aqueous solution of the MB (20 $mg \cdot L^{-1}$).Before to irradiation, the solution was stirred for about 30 min in the dark. Then, 5 mL of suspension was sampled and centrifuged from the reactor at given time intervals, and then analyzed the concentration of the MB supernatant liquid using a UV-vis spectrophotometer (UV-1800PC) at $\lambda_{max¼}$664 nm.

The MB degradation rate constants were calculated by first-order kinetic reaction as follows [18]:

$$\ln (C/C_0) = -kt \quad (1)$$

where C is the concentration of the methylene blue solution, C_0 is the initial concentration of the methylene blue solution, k is the rate of reaction constant, and t is the irradiation time(min).

A recycled photocatalytic experiments on the used catalyst was carried out as following. Briefly, after the reaction of 1st run under UV light irradiation, the suspensions were centrifuged to obtain the photocatalysts, which was washed with anhydrous ethanol and deionized water carefully and then dried in an oven. And then, the photocatalyst was weighed again to add the lost portion. The fresh MB solution was mixed with the used photocatalyst to perform the 2nd run photocatalytic testing. Similarly, the recycled 3rd, 4th, 5th and 6th tests were also performed.

 doi:10.20944/preprints201703.0056.v1

3. Results and discussion

3.1 XRD and BET analysis of the $MgAl_2O_4$ and $Ag/MgAl_2O_4$ samples

Figure 1 shows the XRD pattern of the prepared $MgAl_2O_4$ and $Ag/MgAl_2O_4$powder obtained. In Fig. 1, the observed diffraction peaks at about 2θ=18.98°, 32.24°, 37.05°, 45.97°, 60.60°, 67.24° and 77.29° are compared with the standard JCPDS # 48-0528 data and the formation of pure crystalline phase of $MgAl_2O_4$ samples. The average crystallite size of the prepared sample was calculated using the Scherrer formula [19] and it is about 19 nm. No peaks corresponding to Ag species could be observed in theFig.1 due to the low content of Ag in the samples.

The values of specific surface area estimated from BET measurements yielded as 132 and 145 m^2/g for the S-6 and Ag/S-6 sample, respectively. The average pore diameter of S-6 and Ag/S-6 sample is estimated as 9.7 nm and 6.7 nm, respectively. The low pore diameter of samples may be due to the presence of large amounts of mesopores. High surface area and monomodal pore size distributions are important in catalytic materials measuring the accessibility of reactant molecules.

3.2 SEM and TEM analysis of the $MaAl_2O_4$ and $Ag/MaAl_2O_4$ samples

Figure 2 shows scanning electron microscopy (SEM) of the S-6 (Fig. 2a), Ag/S-6 (Fig. 2b), S-8 (Fig.2c) and Ag/S-8 (Fig.2d)samples, and shows transmission electron microscopy (TEM) images of the S-6(Fig. 2e) and Ag/S-6(Fig. 2f) samples, respectively. The S-6 and Ag/S-6 samples prepared show relatively regular nanorods shape, and the agglomerated rods are well dispersed. However, the S-8 and Ag/S-8 samples prepared show regular nanosheet. Moreover, the average grain size is in the range of 10 to 20 nm from Fig. 2e and 2f. Figure 2b and 2f shows the SEM and TEM micrograph of the Ag/S-6 sample. The nanoparticles distinctly exhibit narrow size distribution with size ranging from 10 to 20

Preprints (www.preprints.org) | NOT PEER-REVIEWED | Posted: 10 March 2017 doi:10.20944/preprints201703.0056.v1

nm. As indicated by the image, one could hardly distinguish the Ag particles from the support because of the low amounts of Ag doping. The results are in good agreement with the XRD analysis.

3.3 DRS and FTIR analysis of the $MgAl_2O_4$ and $Ag/MgAl_2O_4$ samples

The UV-Vis spectra of the $MgAl_2O_4$ and $Ag/MgAl_2O_4$ samples are given in Fig. 3a. The $Ag/MgAl_2O_4$ sample has stronger absorption range than $MgAl_2O_4$ in the whole spectrum range. It shows that due to the induction of the $Ag/MgAl_2O_4$ samples for UV light is more intense due to Ag loading.

Fig.3b shows the FTIR transmittance spectrum of nanocrystalline $MgAl_2O_4$(S-6, S-8) and $Ag/MgAl_2O_4$ (Ag/S-6 and Ag/S-8) samples, respectively. The $MgAl_2O_4$ shows FTIR bands at 656 cm^{-1} and 500 cm^{-1} and these arise due to the stretching vibration of MgO_4 tetrahedral and AlO_6 octahedral groups respectively in the $MgAl_2O_4$ spinel structure [20–22].The bands around 3426 cm^{-1} and 3110 cm^{-1} can be assigned to vibration mode of chemically bonded hydroxyl groups and the deformation vibration of water molecule, respectively [23].The absorption band at 1650 cm^{-1}belongs to free or crystal water [24, 25]. Nanopowder having high surface area promotes rapid adsorption of water from the atmosphere, which is responsible for the formation of peaks in the FTIR spectroscopy. It should be noted that spectra of the samples at 1030 – 1550 cm^{-1} exhibit vibration modes of the groups originating from the organic compounds [26]. The peak at 832 cm^{-1} which is observable in spectrum of the sample obtained after calcination may be attributed to the vibration of NO_3 groups [19].Hence, the observed XRD and FTIR results confirm the formation of $MgAl_2O_4$ nanostructure.

3.4 XPS analysis of the $MgAl_2O_4$ and $Ag/MgAl_2O_4$ samples

Al 2p, Mg 1s, O 1s, Ag $3d_{3/2}$ and C1s X-ray photoelectron spectroscopy (XPS) results of $MgAl_2O_4$

Preprints (www.preprints.org) | NOT PEER-REVIEWED | Posted: 10 March 2017 doi:10.20944/preprints201703.0056.v1

and $Ag/MgAl_2O_4$ sample at pH=6are shown in Fig. 4a-4f.Figure 4 shows the high resolution XPS spectra of the Al peak with Al 2p at 72.96eV (Fig. 4b),O peak with O 1s at 529eV (Fig. 4c). In addition, the Mg peak with Mg 1s at 1303.7eV (Fig. 4d) indicates that the existing form of the sample is $MgAl_2O_4$. No contaminant species were observed within the sensitivity of the technique. Only adsorbed carbon peak with C1s at 282eV (Fig. 4e) on the surface was present in the samples. Figure 4f shows the high resolution XPS spectra of the Ag peak with Ag $3d_{3/2}$ at 372.7eV. It demonstrates that the silver exists in the form of Ag. For the $Ag/MgAl_2O_4$ sample, Table 1 shows the results of measurements from the XPS analysis indicating the atomic ratio of elements Mg/Al/O = 1:2.00:4.24 of the compositions. And the atom ratio of the silver is 0.58%. These results are in good agreement with the XRD analysis, where we have demonstrated the formation of hexagonal crystalline phase of the $MgAl_2O_4$and $Ag/MgAl_2O_4$ samples.

3.5 Photocatalytic activities study

Figure 5 shows the comparison of the photocatalytic activities of the $MgAl_2O_4$ and $Ag/MgAl_2O_4$ samples under UV lamp illumination. Fig. 5a indicates the concentration change of the MB solution over the $MgAl_2O_4$ and $Ag/MgAl_2O_4$ catalysts. For comparison, the photolysis of MB was also carried out under the same condition but without catalyst. Fig. 5a shows that the MB is stable and cannot be easily broken down under UV light irradiation without photocatalysts. Only about 12% MB was degraded under the same irradiation time. Furthermore, it is also show that $Ag/MgAl_2O_4$ displayed higher photoactivity than $MgAl_2O_4$ under UV light irradiation. What's more, the Ag/S-6 catalyst is higher photocatalytic than the Ag/S-8 catalyst. The Ag/S-6 shows the highest activity of 89.6%. This is possibly due to the enhanced light absorption intensity of the Ag/S-6 as showed by UV－Vis absorption spectra in Fig. 3a.The kinetic data for methylene blue degradation under UV-light

Preprints (www.preprints.org) | NOT PEER-REVIEWED | Posted: 10 March 2017 doi:10.20944/preprints201703.0056.v1

illumination were found to follow pseudo first-order reaction [27] as shown in Fig. 5b. The pseudo first-order model was explained by Eq. (1). The rate constants can be obtained from the slope of linear fitting. The apparent first order linear transforms are given in Fig. 5b. The corresponding parameters were presented in Table 2. It shows that all reaction kinetics for the photodegradation of MB over different photocatalysts followed the apparent first-order equation, with higher R^2 values. The obtained apparent rate constants(-k) for the degradation of MB over S-8, S-6, Ag/S-8 and Ag/S-6 are 0.0104, 0.0112, 0.0172 and 0.0189 min^{-1} , respectively. What's more, the enhanced rate constant may play very important roles in improving the photocatalytic degradation activities of Ag/S-6 and Ag/S-8 photocatalysts due to the introduction of Ag. The degradation ratios of the MB solution with the $MgAl_2O_4$ and $Ag/MgAl_2O_4$ samples are shown in Fig. 5c. The results show that the photodegradation ratio of the MB solution with the Ag/S-6 sample is up to 89.6% and that the photodegradation ratios with the Ag/S-8, S-6 andS-8samples are 87.2%, 73.8% and 71.3%, respectively. This implies that the Ag/S-6 sample shows the highest photocatalytic activity among these samples.

3.6 The stability and reusability of the Ag/S-6 catalyst.

An ideal photocatalyst should maintain photochemical stability and reusability under repeated irradiation. To further evaluate the stability and reusability of the Ag/S-6 composite photocatalysts, the recycled photoactivities were measured by running repeated photodegradation reaction of MB over Ag/S-6 for six times under UV light irradiation. The results were shown in Fig. 6. As observed from Fig. 6, it is up to 75.2% after the fifth repetition, which is slightly lower than that (89.6%) with the fresh Ag/S-6 catalyst. It is no distinct activity decline was found after five recycling runs. These results indicate that the composite photocatalyst are relatively stable and no obvious catalyst deactivation.

 doi:10.20944/preprints201703.0056.v1

4. Conclusions

The work has shown that the synthesis of $MgAl_2O_4$ nanoparticles was studied via a simple hydrothermal method with different pH values. The $Ag/MgAl_2O_4$ catalysts were prepared under pH = 6 and 8 by a traditional impregnation strategy. The $Ag/MgAl_2O_4$ catalyst has an attractive photo induction in UV region and remarkable photocatalytic activity towards MB. Higher specific surface area for the $MgAl_2O_4$ catalyst leads to the well dispersion of Ag species on the support, which ensures the access of adsorbates towards the active sites and higher photocatalytic reactivity. The photodegradation ratio of MB over the Ag/S-6 sample is the highest in these $MgAl_2O_4$and $Ag/MgAl_2O_4$ catalysts. The noble metal played a key role in the photocatalytic process. This $Ag/MgAl_2O_4$ catalyst has a significant potential for photocatalytic dye, particularly for the elimination of synthetic dyes compounds.

Acknowledgements

This work was supported financially by the National Nature Science Foundation of China (grant number NSFC-RGC 21061160495); the National High Technology Research and Development Program of China (863 Program) (grant number 2010AA064902); the Major State Basic Research Development Program of China (973 Program) (grant number 2011CB936002); the Excellent Talents Program of Liaoning Provincial University (grant number LR2010090); and the Key Laboratory of Industrial Ecology and Environmental Engineering, China Ministry of Education and the Open Research Fund of Key Laboratory of Subsurface Hydrology and Ecological Effect in Arid Region of

 doi:10.20944/preprints201703.0056.v1

Ministry of Education (grant number 2014G1502033).

References

[1] Martínez-Huitle, C.A.; Brillas, E. . Decontamination of wastewaters containing synthetic organic dyes by electrochemical methods: A general review. *Applied Catalysis B: Environmental.* 2009, 87 (3-4), 105–145.

[2] Xie, Y.; Chen, F.; He, J.; Zhao, J.; Wang, H. . Photoassisted degradation of dyes in the presence of Fe^{3+} and H_2O_2 under visible irradiation. *Journal of Photochemistry and Photobiology A: Chemistry.* 2000, 136(3), 235–240.

[3] Gupta, V.K.; Pathania, D.; Agarwal, S.; Sharma, S. De-coloration of hazardous dye from water system using chemically modified Ficus carica adsorbent. *Journal of Molecular Liquids.* 2012, 174, 86–94.

[4] Ong, S.A.; Toorisaka, E.; Hirata, M.; Hano, T. Biodegradation of redox dye methylene blue by up-flow anaerobic sludge blanket reactor. *Journal of Hazardous Materials.* 2005, 124(1-3), 88–94.

[5] Daud, N.K.; Hameed, B.H. Decolorization of Acid Red 1 by Fenton-like process using rice husk ash-based catalyst. *Journal of Hazardous Materials.* 2010, 176 (1-3), 938–944.

[6] Hoffmann, M.R.; Martin, S.T.; Choi, W.; Bahnemann, D.W. Environmental applications of semiconductor photocatalysis. *Chemical Reviews.*1995 , 95 (1), 69–96.

[7] Li, Y.; Bastakoti, B.P.; Imura, M.; Hwang, S.M.; Sun, Z.; Kim, J.H.; et al. Synthesis of mesoporous TiO_2/SiO_2 hybrid films as an efficient photocatalyst by polymeric micelle assembly. *Chemistry.*

 doi:10.20944/preprints201703.0056.v1

2014, 20 (20), 6027–6032.

[8] Tian, W.; Zhang, C.; Zhai, T.; Li, S.L.; Wang, X.; Liao, M.; et al. Flexible SnO(2) hollow nanosphere film based high-performance ultraviolet photodetector. *Chemical Communications.* 2013, 36 (36), 3739–3741.

[9] Li, X.; Hui, Q.; Shao, D.Y.; Chen, J.J.; Li, C.M.; Cheng, N.P. Stability and electronic structure of $MgAl_2O_4$(111) surfaces: A first-principles study. 2016, *Computational Materials Science*, 112, 8-17.

[10] Artemyeva, E.S; Barinov, D.S; Atitar, F.M.; Murashkina, A.A.; Emeline, A.V.; Serpone, N. Luminescence of photoactivated pristine and Cr-doped $MgAl_2O_4$ spinel. *Chemical Physics Letters.* 2015, 626, 6-10.

[11] An, J.C.; Lee, E.J.; Kim, B.J.; Kim, H.J.; Kim, Y.J.; Shim, J.; et al. Characterization of grapheme nanoplatelets prepared from polyimide-derived graphite. *Materials Letters.* 2015, 161, 321-324.

[12] Mohamed, R.M.; Baeissa, E.S. Mordenite encapsulated with Pt–TiO_2: characterization and applications for photocatalytic degradation of direct blue dye. *J Journal of Alloys and Compounds.* 2013, 558 (5), 68–72.

[13] Abdelaal, M.Y.; Mohamed, R.M. Novel Pd/TiO_2 nanocomposite prepared by modified sol–gel method for photocatalytic degradation of methylene blue dye under visible light irradiation. *Journal of Alloys and Compounds.* 2013, 576 (44), 201–207.

[14] Samanta, T.; Sarkar, S.; Adusumalli, V.N.K.B.; Praveen, A.E. Mahalingam, V. Enhanced visible and near infrared emissions via Ce^{3+} to Ln^{3+} energy transfer in Ln^{3+}-doped CeF_3 nanocrystals (Ln= Nd and Sm). *Dalton Transactions.* 2016, 45 (1), 78-84.

 doi:10.20944/preprints201703.0056.v1

[15] Liu,R.; Wang, P.; Wang, X.; Yu, H.; Yu, J. UV- and visible-light photocatalytic activity of simultaneously deposited and doped Ag/Ag(1)-TiO_2 photocatalyst. *J Physical Chemistry.* 2012, 116 (33), 17721–17728.

[16] Huang, G.; Wang, C.; Xu, S.; Qi, Z.; Lu, C.; Cui, Y. Ag- and Mn-doped ZnInS/ZnS dual-emission quantum dots with zone tunability in the color coordinate. *Nanotechnology.* 2016, 27 (18), 185602.

[17] Bae, D.; Han, K.; Adair, J. Synthesis and microstructure of Pd/SiO_2 nanosized particles by reverse micelle and sol-gel processing. *Journal of Materials Chemistry.* 2002, 12 (10), 3117–3120.

[18] Li, Y.; Wu, W.; Dai, P.; Zhang, L.; Sun, Z.; Li, G. WO_3 and Ag nanoparticle sensitized TiO_2 nanowires: preparation and the enhancement of photocatalytic activity. *RSC Advances.* 2014, 4 (45), 23831–23837.

[19] Motevalian, A.; Salem, S. Effect of glycine–starch mixing ratio on the structural characteristics of $MgAl_2O_4$ nano-particles synthesized by sol–gel combustion. *Particuology.* 2016, 24, 108–112.

[20] Saberi, A.; Golestani-Fard, F.; Sarpoolaky, H.; Willert-Porada,M.; Gerdes, T.; Simon, R. Chemical synthesis of nanocrystalline magnesium aluminate spinel via nitrate-citrate combustion route. *Journal of Alloys and Compounds.* 2008, 462 (1-2), 142-146.

[21] Kutty, P.V.M.; Dasgupta, S. Low temperature synthesis of nanocrystalline magnesium aluminate spinel by a soft chemical method. *Ceramics International.* 2013, 39 (7), 7891-7894.

[22] Alvar, E.N.; Rezaci, M.; Alvar, H.N. Synthesis of mesoporous nanocrystalline $MgAl_2O_4$ spinel via surfactant assisted precipitation route. *Powder Technology.* 2010, 198 (2), 275-278.

[23] Gammard, A.; Babot, O.; Jousseaume, B.; Rascle, M.C.; Toupance, T.; Campet, G. Conductive

 doi:10.20944/preprints201703.0056.v1

F-doped tin dioxide sol-gel materials from fluorinated beta-diketonate tin (IV) complexes. characterization and thermolytic behavior. *Chemistry of Materials*. 2000, 12 (11), 3419-3426.

[24] Banerjee, A.; Das, S.; Misra, S.; Mukhopadhyay, S. Structural analysis on spinel ($MgAl_2O_4$) for application in spinel-bonded castables. *Ceramics International.*2009, 35 (1), 381–390.

[25] Tsuzuki, T.; McCormick, P.G. ZnO nanoparticles synthesised by mechanochemical processing. *Scripta Materialia.* 2001, 44 (8-9), 1731–1734.

[26] Staszak, W.; Zawadzki, M.; Okal, J. Solvothermal synthesis and characterization of nanosized zinc aluminate spinel used in iso-butane combustion. *Journal of Alloys and Compounds*.2010, 492 (1-2), 500-507.

[27] Olad, A.; Behboudi, S.; Entezami, A.A. Preparation, characterization and photocatalytic activity of TiO_2/polyaniline core-shell nanocomposite. *Bulletin of Materials Science.* 2012 , 35 (5), 801–809.

 doi:10.20944/preprints201703.0056.v1

Table Captions:

Table 1 The results of XPS analysis of the Ag/$MgAl_2O_4$ sample.

Table 2 The rate of absorption and photogradation of MB.

 doi:10.20944/preprints201703.0056.v1

Figure Captions:

Figure 1 Typical XRD pattern of the prepared $MgAl_2O_4$samples and Ag/$MgAl_2O_4$ samples.

Figure 2 The SEM images (a=S-6; b=Ag/S-6; c=S-8 and d=Ag/S-8) and TEM images (e=S-6 and f=Ag/S-6) of the $MgAl_2O_4$ samples and the Ag/$MgAl_2O_4$ samples.

Figure 3 The UV-Vis absorption spectra (a) and FTIR spectra (b) of the prepared $MgAl_2O_4$ and Ag/$MgAl_2O_4$ samples.

Figure 4 The whole XPS spectra (a), Al 2p XPS spectra (b), O 1s XPS spectra (c), and Mg1s XPS spectra (d), C1s XPS spectra (e) and Ag $3d_{3/2}$ XPS spectra of the$MgAl_2O_4$sample and Ag/$MgAl_2O_4$samples.

Figure 5 The concentration change of MB under UV light with the $MgAl_2O_4$ and Ag/$MgAl_2O_4$ samples (a); $\ln(C/C_0)$ vs. time for different samples (b) and the photocatolytic degradation ratio of MB with different samples(c).

Figure 6 Cyclic adsorption and photodegradation of MB by the Ag/S-6 sample

Preprints (www.preprints.org) | NOT PEER-REVIEWED | Posted: 10 March 2017 doi:10.20944/preprints201703.0056.v1

Element	Weight (%)	Atom ratio (%)
O K	45.11	58.23
Al K	35.90	27.46
Mg K	15.96	13.73
Ag K	3.03	0.58
Total	100.00	100.00

Preprints (www.preprints.org) | NOT PEER-REVIEWED | Posted: 10 March 2017 doi:10.20944/preprints201703.0056.v1

Sample	Photodegradation	
	$k(10^{-2})$	R^2
S-8	-1.04	0.94
S-6	-1.12	0.95
Ag/S-8	-1.72	0.96
Ag/S-6	-1.89	0.96

Preprints (www.preprints.org) | NOT PEER-REVIEWED | Posted: 10 March 2017 doi:10.20944/preprints201703.0056.v1

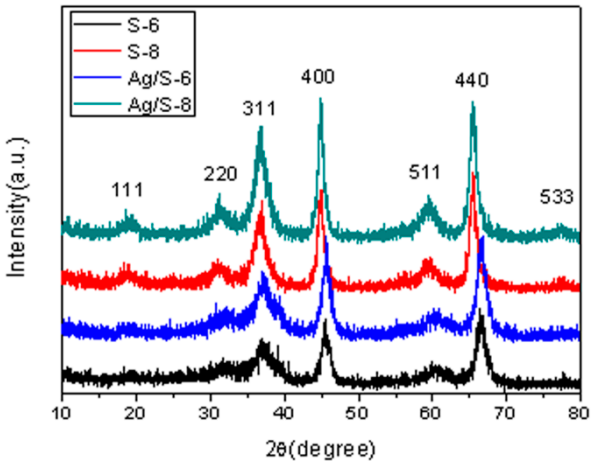

Preprints (www.preprints.org) | NOT PEER-REVIEWED | Posted: 10 March 2017 doi:10.20944/preprints201703.0056.v1

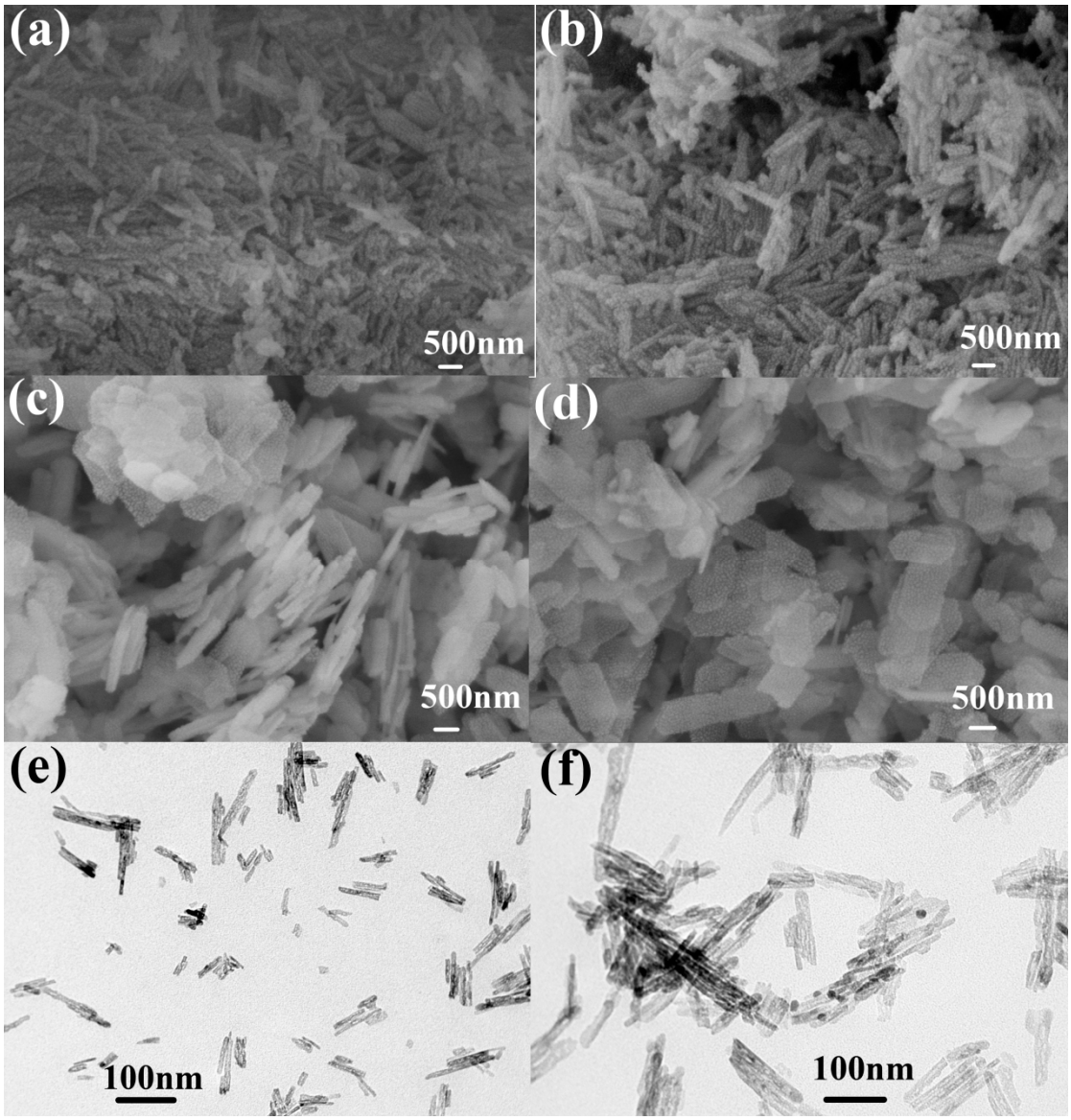

Preprints (www.preprints.org) | NOT PEER-REVIEWED | Posted: 10 March 2017 doi:10.20944/preprints201703.0056.v1

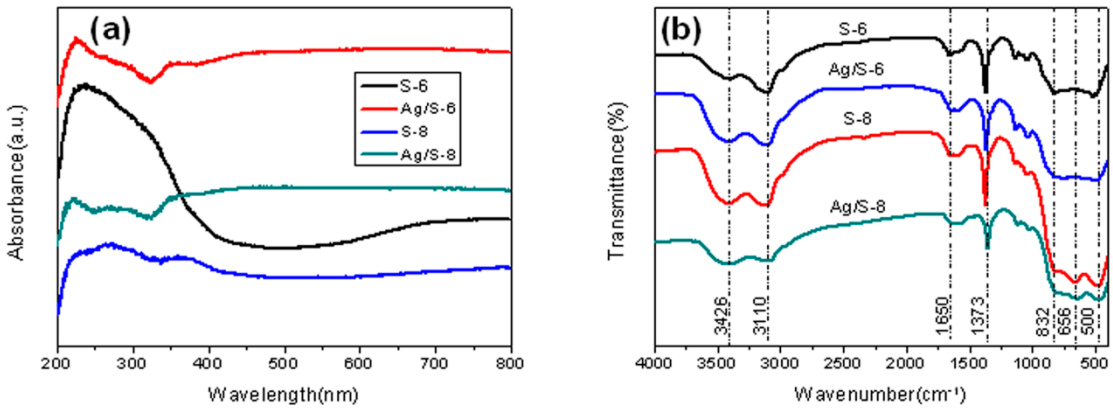

Preprints (www.preprints.org) | NOT PEER-REVIEWED | Posted: 10 March 2017 doi:10.20944/preprints201703.0056.v1

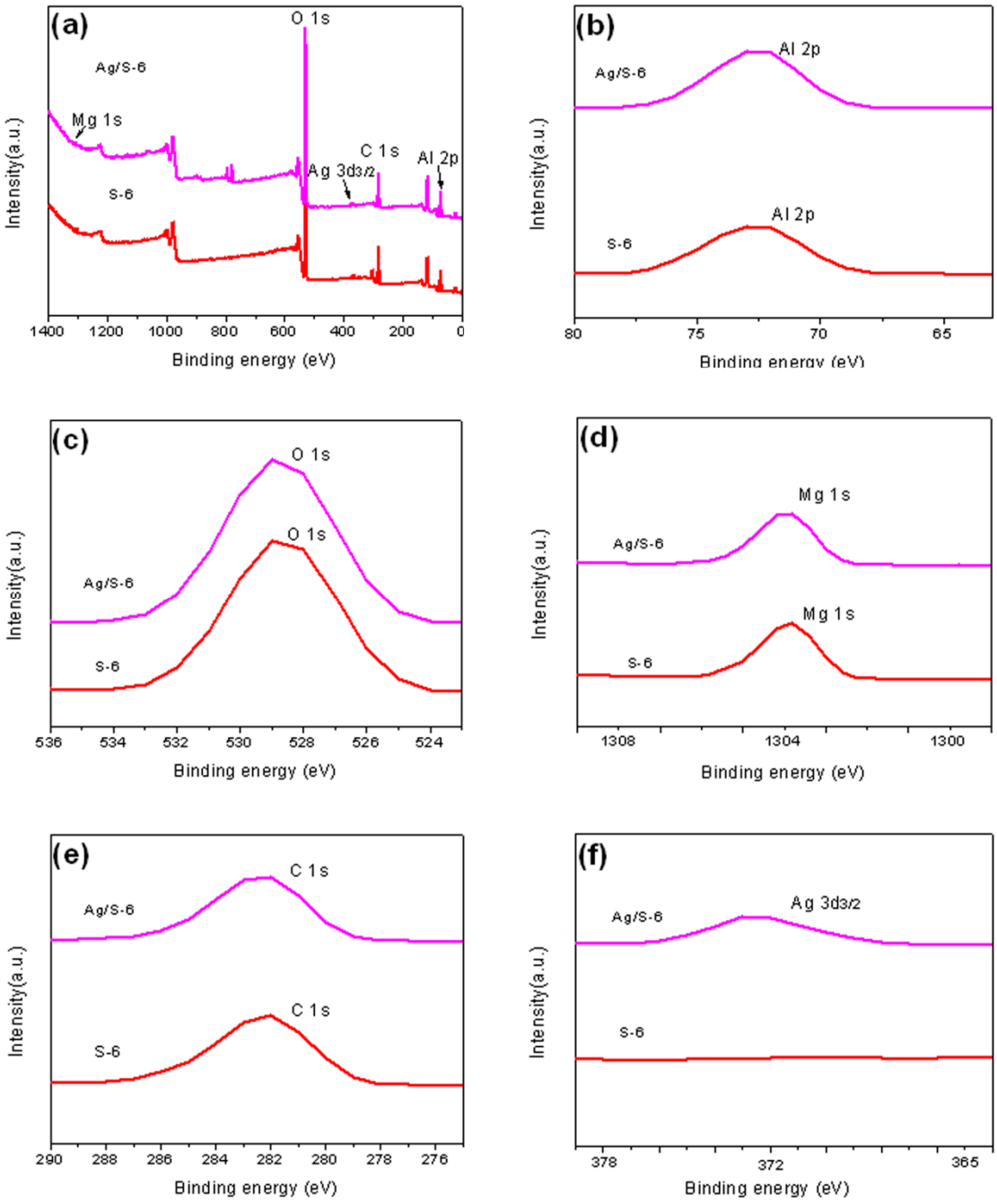

Preprints (www.preprints.org) | NOT PEER-REVIEWED | Posted: 10 March 2017 doi:10.20944/preprints201703.0056.v1

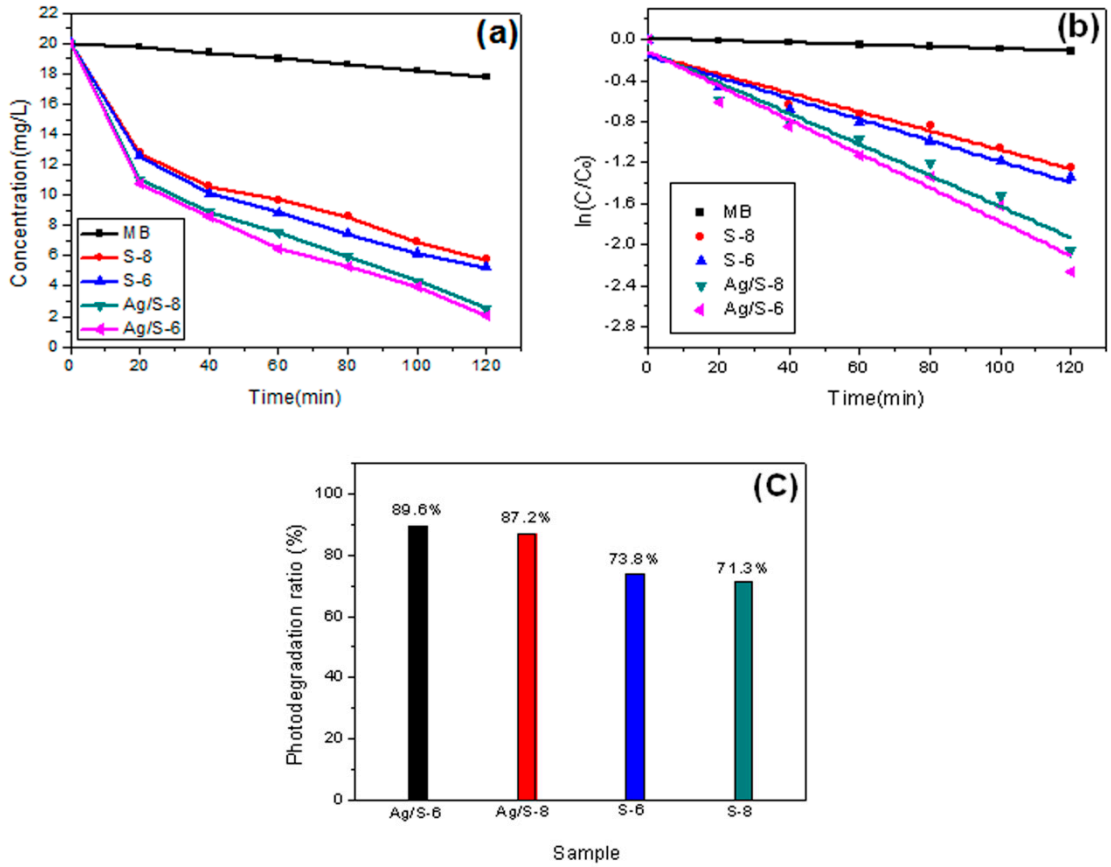

Preprints (www.preprints.org) | NOT PEER-REVIEWED | Posted: 10 March 2017 doi:10.20944/preprints201703.0056.v1